Article type: Full Paper

Growing Oxide Nanowires and Nanowire Networks by Solid State Contact Diffusion into Solution-Processed Thin Films

*Colm Glynn, David McNulty, Hugh Geaney and Colm O'Dwyer**

Dr. Colm Glynn,
Department of Chemistry, University College Cork, Cork T12 YN60, Ireland and Micro-Nano Systems Centre, Tyndall National Institute, Lee Maltings, Cork T12 R5CP, Ireland

Dr. David McNulty,
Department of Chemistry, University College Cork, Cork T12 YN60, Ireland

Dr. Hugh Geaney,
Department of Chemistry, University College Cork, Cork T12 YN60, Ireland

Dr. Colm O'Dwyer,
Department of Chemistry, University College Cork, Cork T12 YN60, Ireland and Micro-Nano Systems Centre, Tyndall National Institute, Lee Maltings, Cork T12 R5CP, Ireland
E-mail: c.odwyer@ucc.ie

Abstract: New techniques to directly grow metal oxide nanowire networks without the need for initial nanoparticle seed deposition or post-synthesis nanowire casting would bridge the gap between bottom-up formation and top-down processing for many electronic, photonic, energy storage and conversion technologies. Whether etched top-down, or grown from catalyst nanoparticles bottom-up, nanowire growth relies on heterogeneous material seeds. Converting surface oxide films, ubiquitous in the microelectronics industry, to nanowires and nanowire networks through addition of extra species with inter-diffusion can provide an alternative deposition method. We show that solution processed thin films of oxides can be converted and recrystallized into nanowires and networks of nanowires by solid-state inter-

diffusion of ionic species from a mechanically contacted donor substrate. $NaVO_3$ nanowire networks on smooth Si/SiO_2 and granular FTO surfaces can be formed by low-temperature annealing of a Na diffusion species containing donor glass to a solution processed V_2O_5 thin film, where recrystallization drives nanowire growth according to the crystal habit of the new oxide phase. This technique illustrates a new method for the direct formation of complex metal oxide nanowires on technologically relevant substrates, from smooth semiconductors, to transparent conducting materials and interdigitated device structures.

1. Introduction

Translating fundamental advances in nanowire (NW) nanoscience into modern technological applications is approaching a state where considerations of cost, stability, performance and direct integration are improving to such a degree, that these building block materials are now part of maturing industrial infrastructures and devices.[1] For semiconducting NWs, we now have a very good understanding and control of their growth, attributes and properties,[2] and some elegant approaches have considerably improved site-selectivity and placement for both bottom-up and top-down modalities.[3] Whether etched top-down, or grown from catalyst nanoparticles bottom-up, NW growth relies on heterogeneous material seeds. Converting surface films to NWs by adding extra species may provide an alternative where growth and crystallization would be related to composition and crystal habit, and oxide NWs, which are difficult to grow and control, could possibly be formed from many oxide thin films.

Growing thin film oxides for electronic and optoelectronic devices is a well-established process, and exquisite control of composition, thickness and coverage is possible using physical vapour methods and also in some cases, solution processing approaches such as dip or spin coating.[4] More complex oxides and ternary oxide films are now the state-of-the-art for high field-effect mobility thin film transistors for display technologies, In-free transparent conducting materials, and as gate dielectrics in CMOS technologies.[5] Complex oxide electronics in the form of thin films and interfaces[6] holds promise for invisible and high power electronics. However, high quality oxide NW formation directly on surfaces, without catalysts and importantly at low temperatures suitable for flexible electronics, still remains a considerable challenge at the new oxide nanomaterials technology level.[7] These NW dispersions have become important for sensing, solar-to-fuel production and also as NW networks for memristor technology[8] and can be adapted for different device components and functional interlayers or coatings in many applications.[1a, 9] NW networks are typically

formed from NWs grown by vapour[9f], physical[9d] and chemical techniques[9h, 10] and largely rely on pre-deposited catalysts nanoparticles for site selective ordered/areal coverage, or by after-growth dispersion or deposition onto choice surfaces. The deposition of NW networks using solution processed methods is becoming more important due to the cost-effectiveness and scalability of these techniques.

Given the importance in developing low temperature, simple methods for high quality oxide NWs in simple and complex crystal structures across any surface coated with an oxide film, we were inspired by the ability of crystalline needles of complex oxide mineral crystals to grow from cracks and oxide surfaces of rough, amorphous stone walls in caves, to see if oxides could grow in NW form from surfaces because of the inclusion of species that cause a certain crystal habit to be followed. In addition, our approach also tried to merge aspects of bottom-up (growth) and top-down (doping, dispersion) processes together to form a design-by-choice NW oxide composition, crystallinity and surface coverage. In this way, doping is achieved after the parent oxide film is first deposited, rather than during deposition as is typically done and the dopant species modifies the composition and resulting crystallinity/shape. No catalysts are used, and the dopant or species diffused into the oxide can be rationally chosen by the ionic composition of the contact source over the oxide film. Ultimately, the oxide thin films of one composition are converted to another choice composition and crystal structure by phase conversion and recrystallization wherever the oxide film exists on a surface, and at very low temperatures compared to typical VLS (vapour-liquid-solid)[11], VSS (vapour-solid-solid) or even SLS (solid-liquid-solid) NW growth methods.

Benefiting from the mature industrial infrastructure for oxide thin film growth[9c, 12] in microelectronics and CMOS facilities, the ability to convert a thin film into an array of high quality oxide NWs without pre-placed catalysts by phase conversion using to-down

solid state contact diffusion provides an elegant way of high surface area coverage of a wide variety of oxide NW compositions. Inter-diffusion processes can be used to grow a wide range of oxide NW structures which can be judiciously chosen by the initial oxide thin film composition and the nature of mobile species in the contact source.[13]

Here, we detail this new contact diffusion phase conversion and low temperature oxide NWs and NW network growth method using a solution-processed vanadium pentoxide (V_2O_5) thin film and a physically-contacted glass containing the donor species. The surface contacted glass provides Na species to the V_2O_5 thin film which facilitates the formation of α-$NaVO_3$ NW networks through inter-diffusion, sensitively monitored by Raman scattering spectroscopy and electron microscopy. The combination of solution processed techniques to form a thin film of one oxide composition, and top down solid state inter-diffusion processes, phase change and recrystallization opens up a new avenue of research into oxide NW growth, doping[14] and NW shape and physical property control across surfaces, substrates and device structures directly.

2. Results and Discussion

The contact inter-diffusion technique, top-down into metal oxide thins films to form phase converted oxide NWs, is outlined in the schematic of **Figure 1** (a). Initially, a thin film of a-V_2O_5 is dip-coated onto the substrate with uniform thickness, in this case of ~ 10 nm – 15 nm per layer.[13a, 15] Both the donor glass and thin film surfaces must be clean, with low roughness (<1 nm rms) and free of defects to ensure good interfacial contact to enable inter-diffusion. Coatings such as FTO or ITO act as diffusion barriers to ionic mobility, preventing diffusional movement elemental species, which can occur if a glass substrate is used[13a], and so we detail an approach for diffusional incorporation of ionic species top-down in order

to cause a phase change in the thin dip-coated film coated on ITO, FTO or oxide-coated semiconductor substrates. A clean borosilicate donor glass containing the mobile ionic (in this case Na) species is contacted with the surface of the a-V_2O_5 thin film and pressure is applied to keep intimate contact during annealing. Thermal annealing parameters, temperature and time, were refined between different a-V_2O_5 thickness samples to initiate and maintain phase conversion to the 'transparent phase' – the transparent phase is the region on the substrate that defines the resulting NW network.

A contact diffusion-formed transparent region is visible in the centre of a single layer of a-V_2O_5 on an FTO substrate in the optical image of Figure 1 (b) after thermal annealing. The contacted glass had a distinctive shape, which is evident on the surface of the V_2O_5 thin film after the inter-diffusion processes occurred during annealing, and so the regions of interest can be readily identified. For this sample, consisting of a single a-V_2O_5 layer on FTO, the transparent region was formed during a 72 h thermal anneal at 300 ^oC. A long thermal annealing period was applied to enable the contact diffusion process at this temperature, based on previous estimations of solid state diffusivities from borosilicate glass into a-V_2O_5 thin films.[13a] SEM images of the surface of the contacted region in Figure 1 (c) shows the conversion of the thin film to a well-dispersed interconnected α-$NaVO_3$ NW network across the surface of the FTO. The FTO substrate has a granular morphology, but we stress that it has conformal coverage by the dip-coated V_2O_5 thin film that is ~10× thinner with an order of magnitude lower rms roughness (see Supporting Information Figure S1). Secondary electron intensity from the underlying FTO substrate ensures the grains are visible through the continuous, lower conductivity a-V_2O_5 thin film.

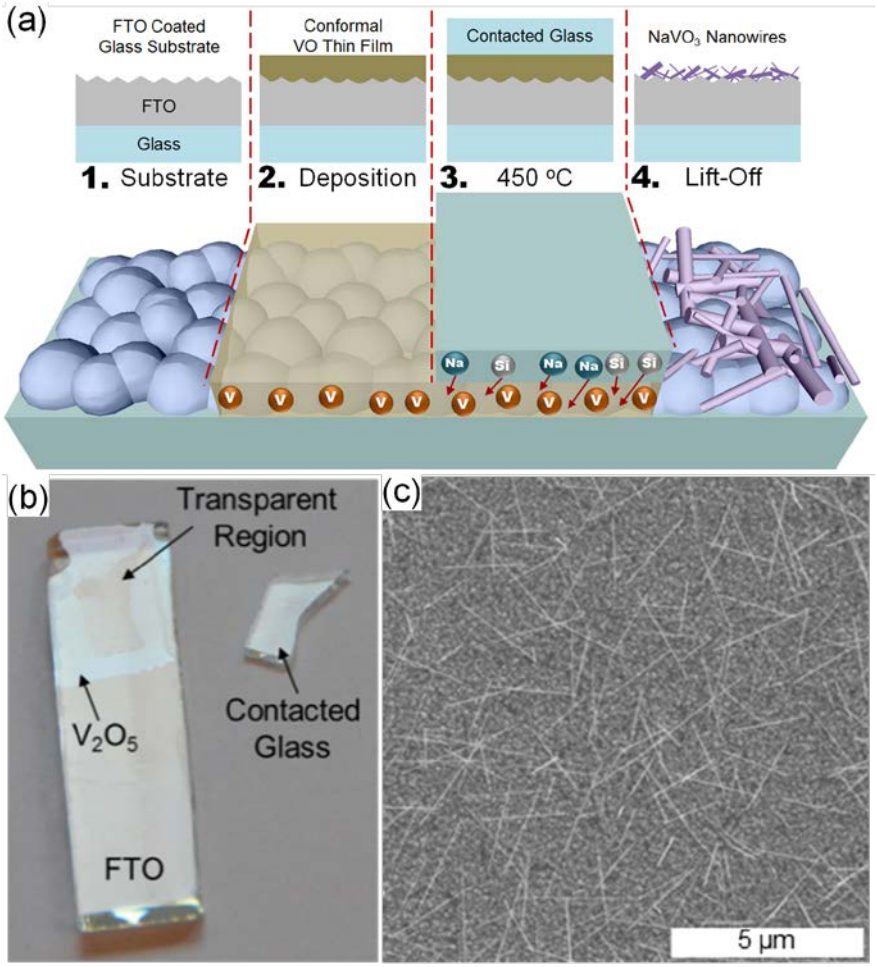

Figure 1. (a) Schematic of deposition technique for contact diffusion inter-diffusion process. (b) Optical image after thermal annealing of an orthorhombic V_2O_5 thin film on FTO with a contact diffused area in the centre and the contacted glass used and (c) SEM image of contact diffused area showing formation of NW network.

For inter-diffusion of a-V_2O_5 thin films to form α-$NaVO_3$ layers when deposited directly onto glass substrates, a thermal anneal at 300 ºC for 12 h is sufficient for a conformal coating.[13a] In the contact inter-diffusion process a greater thermal energy or longer annealing time is required to allow diffusion across the contacted interface between the glass and the oxide film-on-substrate surfaces. The NWs formed in the transparent region of Figure 1 (b) are spread across the surface of the region in differing concentrations, as shown in Figure 1 (c). As outlined in Supporting Information Figure S2, the outer areas of the NW-containing region typically have the highest concentration of NWs.

To form a more uniform NW network, the thickness of the a-V_2O_5 layer was increased to ~30 nm by dip-coating 3 layers in succession. The thicker a-V_2O_5 layer ensures a larger amount of V species available for the formation of the α-$NaVO_3$ NWs. The annealing temperature was increased to 450 ^oC and the annealing time set to 6 h, decreasing the NW network formation time.

The morphology of the NW network for a contact-diffused sample with an initial 30 nm thick a-V_2O_5 thin film annealed at 450 ^oC for 6 h is shown in **Figure 2**. The SEM images in Figure 2 (a, b) show the large NW network coating that forms on the surface of the outer contacted region. Nodes are apparent on the surface of the NW network and a higher SEM magnification of these nodes is shown in Figure 2 (c). NWs radially spread from a centre mass within these nodes resulting in a larger localised NW concentration. Formation of the nodes is attributed to the presence of a surface defect or raised region on the substrate/a-V_2O_5 thin film where the NWs radially grew from due to a localised change in the pressure with the donor glass substrate. However, the overall deposit shows a very high and relatively uniform dispersion of NWs on the FTO surface, each composed of the mixed metal oxide $NaVO_3$, forming a NW networked region.

A higher magnification SEM image of the NWs is shown in Figure 2 (d). The NWs have a uniform morphology and appear to be ribbon shaped with a larger NW diameter than thickness. The fibrous morphology of the NWs is common in both vanadium oxide nanomaterials[16] and $NaVO_3$ structures.[17] In Figure 2 (e, f) SEM images of smaller $NaVO_3$ rods within the centre of the contact diffusion-formed NW network regions are shown. In these areas the formation of larger shards, see the Supporting Information Figure S4, surrounded by regions of rods can be seen on the surface. Seeded growth of NWs is a commonly used method for the preparation of networks[18]. It was previously demonstrated that dip-coated thin films of a-V_2O_5 have an in-plane morphology composed of “flakes” or

grains of amorphous vanadium oxide. The SEM images of Figure 2 (e, f) shows that a-V_2O_5 grains from the dip-coated thin film are the 'seeds', where recrystallization due to inter-diffusion starts to occur, as these grains are within the thin film that conformally coats the granular FTO substrate. The small spaces between the undulating FTO grains ensure that voids form between the thin films and the contacted glass, allowing the growth of the NWs from the a-V_2O_5. Shown in Figure 2 (f) and highlighted with false colour images in the inset, the tail of the rods can be seen protruding from the surface of the thin film suggesting that their formation is seeded from the changes to the phase and crystal structure of the surface film, and continue to grow via recrystallization from inter-diffusion from the donor substrate that supplies the Na species.

Raman scattering spectroscopy was used to examine the different regions on the surface of the NW network region. The Raman scattering spectra for the V_2O_5 and NW regions formed from a single layer of a-V_2O_5 is shown in the Supporting Information Figure S3, where the annealed V_2O_5 thin film forms the characteristic orthorhombic crystal structure expected from V_2O_5[15b] and the NW network region shows the formation of the characteristic vibrational modes for α-$NaVO_3$.[19] However, the modes are shifted from 918 cm^{-1} and 955 cm^{-1}, to 925 cm^{-1} and 951 cm^{-1} respectively, which are related to size and stress effects on the crystalline α-$NaVO_3$ phase that forms within the glassy matrix, a common effect for NW systems due to phonon confinement and scattering.[20] In comparison, the Raman vibrational spectra for two different regions of the NW network formed with 30 nm (3 layers) of a-V_2O_5 annealed at 450 ^oC are shown in Figure 2 (g) with orthorhombic V_2O_5 as a comparison. The observation of the 954 cm^{-1} and 918 cm^{-1} modes indicative of α-$NaVO_3$ are present in the Raman spectra[19, 21] with no evidence of mode shifting due to stresses within the crystal structure, boundary scattering or quantum confinement of phononic modes. The

thicker 30 nm initial V_2O_5 thin film coupled with a shorter and higher temperature annealing (450 °C for 6 h) step formed an α-$NaVO_3$ NW network on the surface of the FTO substrate.

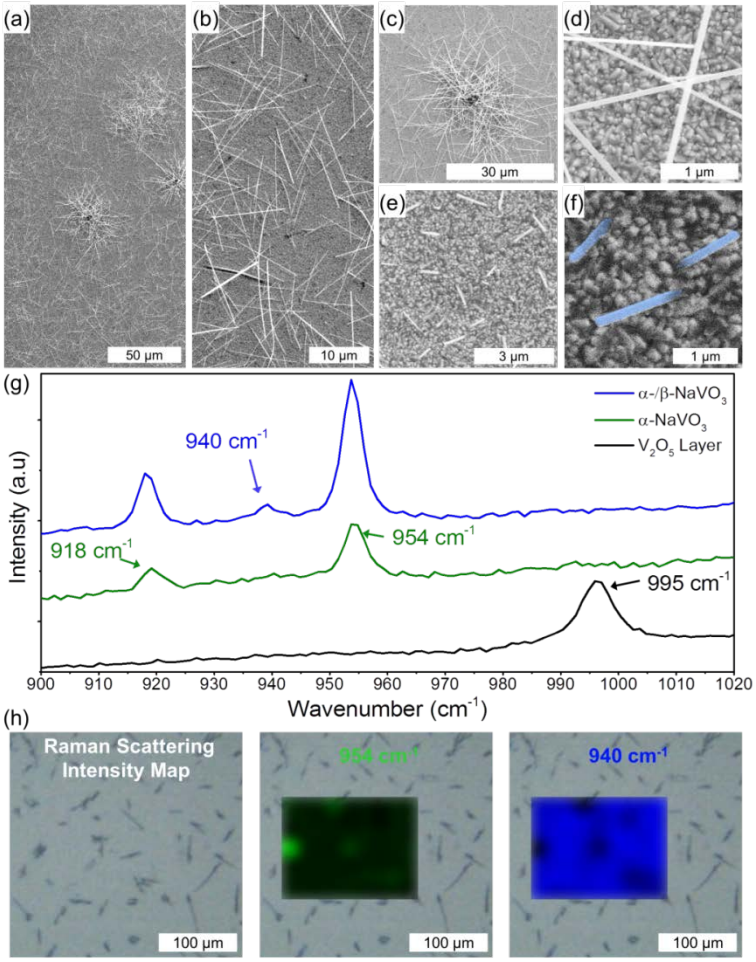

Figure 2. SEM images of the surface of a transparent region formed on a 3 layer thick a-V_2O_5 thin film annealed at 450 °C for 6 h. SEM images of (a-b) high concentration region of NWs with presence of NW nodes. (c) SEM image of a NW node and (d) higher magnification image of individual NWs. (e-f) SEM images from the inner area of the NW region showing rods formation on the FTO surface. (g) Raman scattering spectra of V_2O_5 thin film and two different areas of the NW region showing evidence of the formation of α-$NaVO_3$ within the NWs. (h) Raman scattering spectroscopy intensity map highlighting the areas where the 954 cm^{-1} and 940 cm^{-1} modes increase in intensity.

The presence of a secondary vibrational mode at 940 cm^{-1} in the blue coloured spectrum of Figure 2 (g) is attributed to the presence of β-$NaVO_3$ with the α-$NaVO_3$ within the NWs[17, 19, 21] at specific areas within the network. Raman intensity mapping of the 940 cm^{-1} (corresponding to β-$NaVO_3$) and 955 cm^{-1} (corresponding to α-$NaVO_3$) modes, shown in Figure 2 (h), demonstrates that the α-$NaVO_3$ (955 cm^{-1} vibrational mode) is directly

from the larger NWs while the β-$NaVO_3$ (940 cm^{-1} mode) is specific to the areas between these shards where the rods formed - where full crystallization to NWs has not happened.[19, 21]

It is known from investigation of these same $NaVO_3$ phases in large mineral deposits in underground vents and caves, that the formation of α-$NaVO_3$ occurs at higher temperatures after β-$NaVO_3$ is formed.[21] On the nanoscale, the spectroscopic evidence for the β-$NaVO_3$ is found where the structures recrystallize out as larger rods or remain as thin film in this phase. With sufficient ionic species from the donor contact source, an insufficient thermal energy prevents further phase change to needle-like α-$NaVO_3$ NWs. An average diffusion constant of $D = 3.5 \times 10^{-15}$ cm^2 s^{-1} was calculated for the species inter-diffusing from planar glass to an a-V_2O_5 thin film directly dip-coated onto the surface at the processing temperature of 450 °C. The ionic species inter-diffusion process is rapid and occurs much faster than the crystallisation of the a-V_2O_5 to orthorhombic V_2O_5. β-$NaVO_3$ occurs prior to the formation of orthorhombic V_2O_5 when glass is contacted (confirmed by Raman scattering), and the evolution from β-$NaVO_3$ to α-$NaVO_3$ occurs over a longer (subsequent) annealing time during inter-diffusion. The Raman scattering spectra of the pre- and post-annealed donor glass is shown in the Supporting Information Figure S5, confirming no evidence of V species diffusion to the glass to form a detectable crystalline phase during annealing, nor delamination of the material coated onto the substrate. In Supporting Information Figure S6, we demonstrate that different sized NWs can be prepared and their formation localised by etching into the glass diffusion source, thereby removing intimate contact with the thin films substrate. The resulting formation of larger nanostructures is achieved, however, a large-scale connected network is not realised which limits the application of the technique suggesting that a planar donor surface is required for high concentration $NaVO_3$ NW networks.

To examine the structure and morphology of the NWs formed through the contact diffusion mechanism, and how the underlying roughness of the thin film-coated substrate discussed earlier affects nucleation and recrystallization, thin films of a-V_2O_5 were dip-coated onto the surface of Si_3N_4 membranes and annealed at 450 ^oC for 6 h while contacted to a cleaned glass piece. The TEM and AFM image in **Figure 3** (a) shows the surface of an orthorhombic V_2O_5-coated Si_3N_4 surface after annealing without glass contacting. The thin film surface is composed of individual V_2O_5 grains resulting in a smooth and uniform coating. TEM and AFM images of the a-V_2O_5 thin film deposited on Si_3N_4 prior to annealing are shown in Supporting Information Figure S7 with more detailed analysis on these thin films available elsewhere.[15b] The TEM image in Figure 3 (b) shows the structures formed on the same Si_3N_4 grid with donor glass in contact with the a-V_2O_5 during annealing. The surface is composed of large quantities of NWs, and other nanostructured materials, such as shards and sheets, which we find are typical when recrystallization occurs between smooth surfaces, even when the thin oxide film itself is granular.

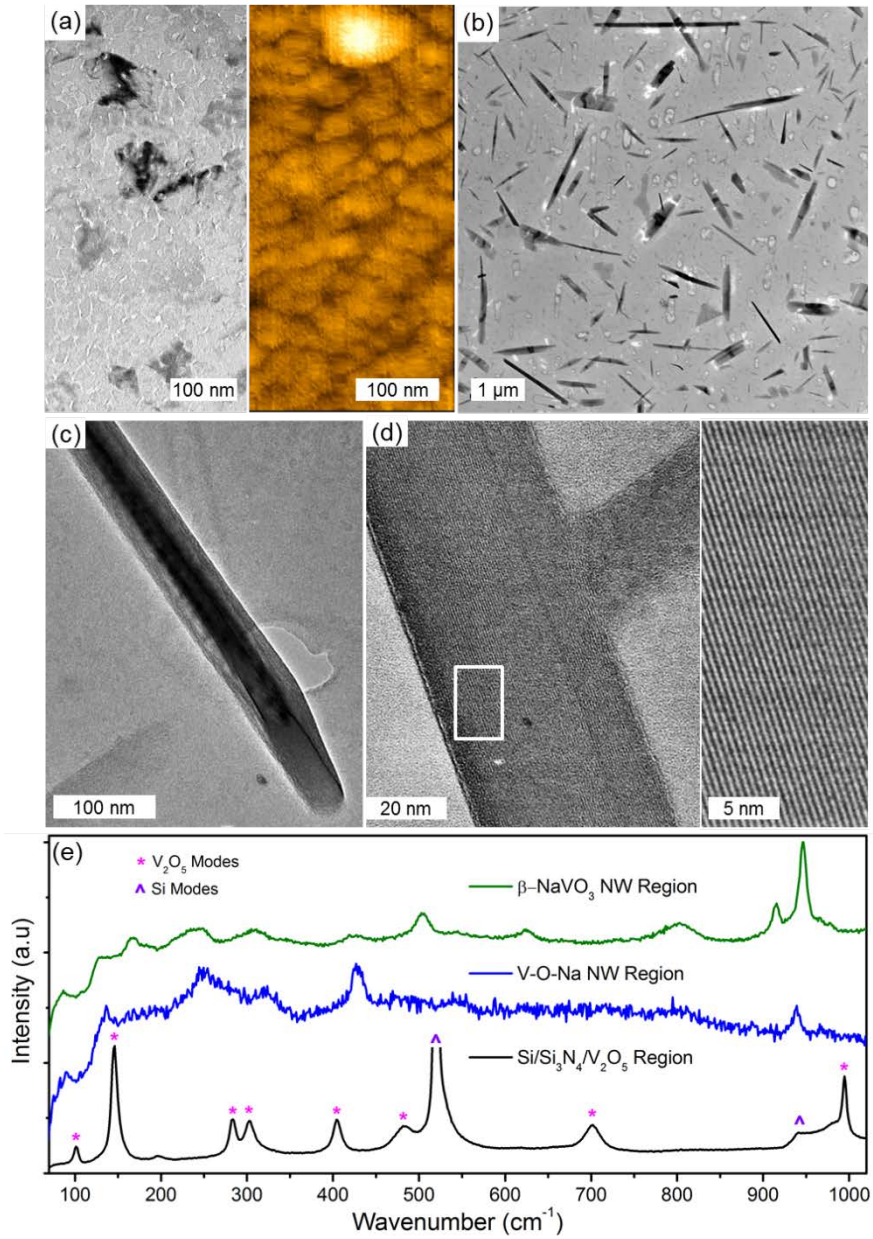

Figure 3. (a) HRTEM and AFM images of annealed solution-processed orthorhombic V_2O_5 thin film on Si_3N_4 membranes. (b) TEM image of the nanostructures formed on a contact diffused surface deposited on a Si_3N_4 TEM grid. (c) HRTEM image of a NW displaying a dense interior and (d) crystalline structure. (e) Raman scattering spectra of contact-diffused regions indicating vibrational modes for orthorhombic V_2O_5 on Si and those corresponding to β-$NaVO_3$ and V-O-Na materials.

A singular long NW is shown in the HRTEM image of Figure 3 (c). The interior of the NW is darker denoting a denser inner surface while the surrounding material is less dense. This type of deposit can be seen in many areas of the low magnification image of Figure 3 (b). These nanostructures formed on the Si_3N_4 surface through inter-diffusion are crystalline

in nature as evidenced by the TEM images in Figure 3 (d), with well-defined inter-planar spacings apparent. Raman scattering spectroscopy was performed on the contact-diffused Si_3N_4 membrane after annealing with the spectra shown in Figure 3 (e) compared to orthorhombic V_2O_5 thin films deposited on Si/Si_3N_4. In the Si_3N_4 free-standing window regions containing the NW structures, evidence of different vibrational modes is found. Raman vibrational modes corresponding to the formation of the β-$NaVO_3$ phase is present in the NW regions, however unknown spectra are also present within these regions which match that of neither orthorhombic V_2O_5 nor α-/β-$NaVO_3$. The unknown spectra shown in Figure 3 (e) is attributed to the formation of a different V-O-Na structure. The effect of the smooth Si_3N_4 surface and the fragility of the TEM grid during glass contacting is attributed to the formation of nanostructures not matching that of known $NaVO_3$ materials.

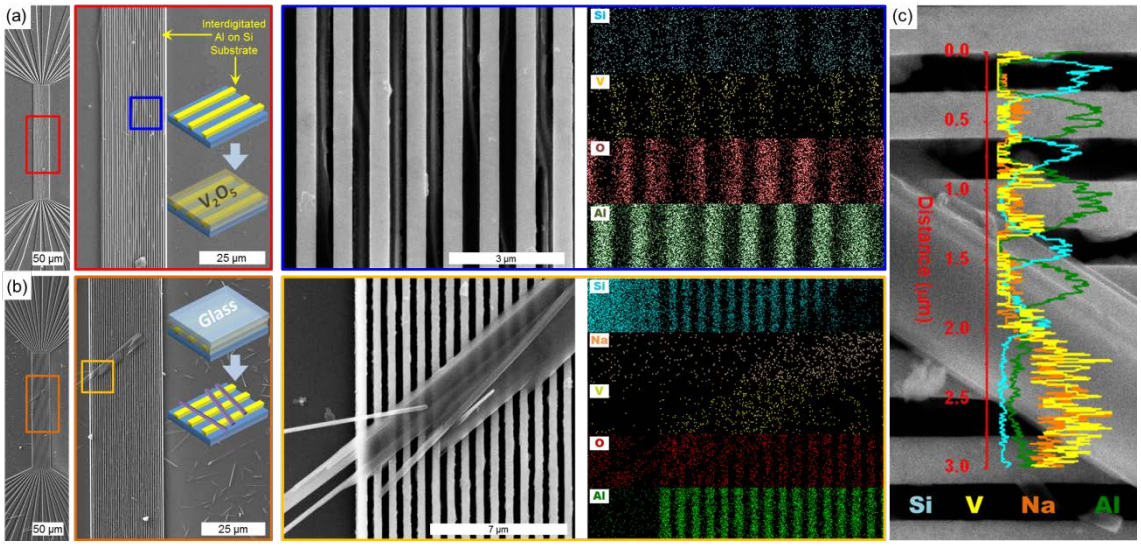

Figure 4. SEM images comparing (a) V_2O_5 thin film and (b, c) $NaVO_3$ contact diffused NW formation on interdigitated Al layers on Si/SiO_2 substrates. EDX mapping shows the distribution of Si, O, V, Al and Na on the surfaces.

This process also provides an alternative to NW deposition or casting protocols and allows direct NW formation on device-like structures, demonstrated in **Figure 4** (a-c). An Si/SiO_2 substrate with interdigitated Al electrodes was dip-coated with a layer of a-V_2O_5. Annealing was performed on both uncontacted and contacted device structures to

recrystallize the film to NWs. In the uncontacted samples the V_2O_5 thin film uniformly coats the Si/SiO_2 substrate and Al interdigitated electrodes, while inter-diffusion processes from contacted samples allowed the formation $NaVO_3$ NWs across this particular device structure.

EDX mapping of all V, Si, Al, Na and O elements confirms uniform coating of the orthorhombic V_2O_5 thin film when uncontacted. Detailed EDX mapping and supplementary images are included in Supporting Information Figures S8 – S11. EDX analysis confirms that Na was not found in the uncontacted samples, and the elemental distributions are consistent with conformal coating of the device structure and substrate. The EDX map for the $NaVO_3$ NWs grown form the V_2O_5 films on the Al electrodes shows a high concentration of both V and Na localised to the NWs, above the Si and Al-containing device substrate. This confirms that the diffusion of Na species into the a-V_2O_5 film occurs throughout the film, and recrystallization into NWs accommodates most of the V, O and Na mass as NWs. The underlying surface has significantly reduced V species because of its localised incorporation into the NW structures with the formation of NWs and other structures facilitated under the right conditions.

3. Conclusions

In summary, we have developed a new technique for the formation of oxide NWs on surface and directly on device structures using a contact diffusion deposition technique. Low temperature induced inter-diffusion between a mechanically contacted donor glass containing Na species, and a solution processed a-V_2O_5 thin film was shown to facilitate the formation of $NaVO_3$ NWs and nanostructures on a variety of surfaces, from smooth Si/SiO_2 to rougher granular FTO morphologies and interdigitated metal electrodes. It was shown that Na diffuses from the contacted donor glass to the a-V_2O_5 thin film where the amorphous grains

act as “seeds” for NW growth, negating the need for a separate nanoparticle seed deposition step.

The contact diffusion mechanism between the a-V_2O_5 thin film and a borosilicate donor glass demonstrates the capability of solid-state inter-diffusion processes for forming NW networked morphologies of $NaVO_3$ transparent materials across various surfaces, negating the requirement for extra casting protocols and techniques post-NW production. This technique can potentially be expanded to directly form single crystal NWs and NW networks of complex oxide phases from a range of oxide thin films contacted with donor substrate with alternative ionic species that can be driven by thermal inter-diffusion. In future studies it will be applied for the possible next-generation formation of cation-intercalated metal oxides for use in thin film batteries, smart window electrochromics, networked NWs for memristors and many other applications that require high surface area NW networks of metal oxides, with NW structure and morphology dictated by the crystal habit of the oxide phase.

4. Experimental

For contact diffusion deposition, dip-coated thin films of amorphous V_2O_5 (a-V_2O_5) were deposited onto 350 nm thick fluorine-doped tin oxide (FTO) coated glass substrates with a 1000:10:1 (IPA : Alkoxide : H_2O) precursor solution. The initial a-V_2O_5 thin films were dip-coated using a PTL-MM01 desktop dip coater at a constant withdraw rate of 2.5 mm/s. For thicker a-V_2O_5 thin films, multiple layers were successively dip-coated after allowing sufficient time for the previous layer to dry. Clean borosilicate glass (composition: SiO_2 72.20%, Na_2O 14.30%, CaO 6.40%, MgO 4.30%, Al_2O_3 1.20%, K_2O 1.20%, SO_3 0.30% and Fe_2O_3 0.03%) was placed on the surface of the fully hydrolysed as-deposited a-

V_2O_5 thin film and weighted down to ensure equalised and intimate contact between the glass and a-V_2O_5 thin film. UV-O_3 cleaning of the a-V_2O_5 and glass surfaces using a Novascan UV-O_3 system was conducted for 1 h prior to contacting to ensure a clean surface. Annealing in air at 300 ^oC was performed in a conventional oven for 72 h. An enclosed furnace was used for annealing at 450 ^oC. For smaller sample sizes, such as Si_3N_4 TEM grids, contacting was performed by sandwiching between two glass pieces for ensuring uniform pressure across the surface. Contact diffusion was also performed on interdigitated Al contacts deposited on Si/SiO_2 wafers using the same dip-coating and contacting parameters.

The thin film surface morphology was examined with SEM performed on an FEI Quanta 650 FEG high resolution SEM with operating voltages of 10-20 kV equipped with an Oxford Instruments X-MAX 20 large area Si diffused EDX detector. AFM analysis was performed on a Park XE-100 AFM system in non-contact mode with SSS-NCHR enhanced resolution tips, the XY and Z resolution are ~ 2 nm and 0.05 nm respectively. Raman scattering spectroscopy was collected on a Renishaw InVia Raman spectrometer using a 514 nm, 30 mW laser source. Spectra were collected and focused onto the samples using a 50× objective lens. Mapping of the intensity of Raman vibrational modes was accomplished using a computerised movable microscope stage.

HRTEM analysis of the contact-diffused NWs was performed using a JEOL 2100 high resolution TEM operating at 200 kV. Single layers of a-V_2O_5 thin films were dip-coated onto the surface of 15 nm thick Si_3N_4 membrane windows, and contacted to the glass as the ionic species source as described above. Device structures were made using standard photolithography and metallization process, to form interdigitated structure of 500 nm wide Al lines on Si/SiO_2.

Supporting Information

Supporting Information is available from the Wiley Online Library or from the author.

Acknowledgments

C.G. acknowledges the support of the Irish Research Council under award RS/2011/797. This work was also supported by Science Foundation Ireland (SFI) under the National Access Programme (NAP 417), and through an SFI Technology Innovation and Development Awards under contracts no. 13/TIDA/E2761 and 15/TIDA/2893. This publication has also emanated from research supported in part by a research grant from SFI under Grant Number 14/IA/2581.

References

[1] a) Li, Y.; Qian, F.; Xiang, J.; Lieber, C. M., *Mater. Today* **2006,** *9,* 18; b) Yang, P.; Yan, R.; Fardy, M., *Nano Lett.* **2010,** *10,* 1529.

[2] a) Xia, Y.; Yang, P.; Sun, Y.; Wu, Y.; Mayers, B.; Gates, B.; Yin, Y.; Kim, F.; Yan, H., *Adv. Mater.* **2003,** *15,* 353; b) Duan, X.; Huang, Y.; Agarwal, R.; Lieber, C. M., *Nature* **2003,** *421,* 241; c) Yang, P.; Lieber, C. M., *Science* **1996,** *273,* 1836.

[3] a) Cui, Y.; Wei, Q.; Park, H.; Lieber, C. M., *Science* **2001,** *293,* 1289; b) Mårtensson, T.; Svensson, C. P. T.; Wacaser, B. A.; Larsson, M. W.; Seifert, W.; Deppert, K.; Gustafsson, A.; Wallenberg, L. R.; Samuelson, L., *Nano Lett.* **2004,** *4,* 1987; c) Boukai, A. I.; Bunimovich, Y.; Tahir-Kheli, J.; Yu, J. K.; Goddard, W. A., 3rd; Heath, J. R., *Nature* **2008,** *451,* 168.

[4] Grosso, D., *J. Mater. Chem.* **2011,** *21,* 17033.

[5] a) Jiang, J.; Li, Y.; Liu, J.; Huang, X.; Yuan, C.; Lou, X. W., *Adv. Mater.* **2012,** *24,* 5166; b) Freund, H.-J.; Pacchioni, G., *Chem. Soc. Rev.* **2008,** *37,* 2224; c) Chueh, C.-C.; Li, C.-Z.; Jen, A. K. Y., *Energy Environ. Sci.* **2015,** *8,* 1160; d) Si Joon, K.; Seokhyun, Y.; Hyun Jae, K., *Jpn. J. Appl. Phys.* **2014,** *53,* 02BA02; e) Lee, D. H.; Chang, Y. J.; Herman, G. S.; Chang, C. H., *Adv. Mater.* **2007,** *19,* 843; f) Lee, W.-J.; Park, W.-T.; Park, S.; Sung, S.; Noh, Y.-Y.; Yoon, M.-H., *Adv. Mater.* **2015,** *27,* 5043; g) Jiang, Q.; Feng, L.; Wu, C.; Sun, R.; Li, X.; Lu, B.; Ye, Z.; Lu, J., *Appl. Phys. Lett.* **2015,** *106,* 053503; h) Thomas, S. R.; Pattanasattayavong, P.; Anthopoulos, T. D., *Chem. Soc. Rev.* **2013,** *42,* 6910; i) Grill, A.; Gates, S. M.; Ryan, T. E.; Nguyen, S. V.; Priyadarshini, D., *Appl. Phys. Rev.* **2014,** *1,* 011306.

[6] a) Osborne, I.; Lavine, M.; Coontz, R., *Science* **2010,** *327,* 1595; b) Rondinelli, J. M.; Poeppelmeier, K. R.; Zunger, A., *APL Mater.* **2015,** *3,* 080702.

[7] a) Kim, M.-G.; Kanatzidis, M. G.; Facchetti, A.; Marks, T. J., *Nat. Mater.* **2011,** *10,* 382; b) Arias, A. C.; MacKenzie, J. D.; McCulloch, I.; Rivnay, J.; Salleo, A., *Chem. Rev.* **2010,** *110,* 3; c) Klamchuen, A.; Suzuki, M.; Nagashima, K.; Yoshida, H.; Kanai, M.; Zhuge, F.; He, Y.; Meng, G.; Kai, S.; Takeda, S.; Kawai, T.; Yanagida, T., *Nano Lett.* **2015,** *15,* 6406.

[8] a) Bellew, A. T.; Bell, A. P.; McCarthy, E. K.; Fairfield, J. A.; Boland, J. J., *Nanoscale* **2014,** *6,* 9632; b) Nirmalraj, P. N.; Bellew, A. T.; Bell, A. P.; Fairfield, J. A.; McCarthy, E. K.; O'Kelly, C.; Pereira, L. F. C.; Sorel, S.; Morosan, D.; Coleman, J. N.; Ferreira, M. S.; Boland, J. J., *Nano Lett.* **2012,** *12,* 5966; c) Kuykendall, T.; Ulrich, P.; Aloni, S.; Yang, P., *Nat. Mater.* **2007,** *6,* 951.

[9] a) Kang, M.-G.; Joon Park, H.; Hyun Ahn, S.; Jay Guo, L., *Sol. Energ. Mat. Sol. Cells* **2010,** *94,* 1179; b) Hu, L.; Kim, H. S.; Lee, J.-Y.; Peumans, P.; Cui, Y., *ACS Nano* **2010,** *4,* 2955; c) Lee, J.-Y.; Connor, S. T.; Cui, Y.; Peumans, P., *Nano Lett.* **2008,** *8,* 689; d) O'Dwyer, C.; Szachowicz, M.; Visimberga, G.; Lavayen, V.; Newcomb, S. B.; Torres, C. M. S., *Nat. Nanotechnol.* **2009,** *4,* 239; e) Nakayama, Y.; Pauzauskie, P. J.; Radenovic, A.; Onorato, R. M.; Saykally, R. J.; Liphardt, J.; Yang, P., *Nature* **2007,** *447,* 1098; f) Arnold, S. P.; Prokes, S. M.; Perkins, F. K.; Zaghloul, M. E., *Appl. Phys. Lett.* **2009,** *95,* 103102; g) Mikyung, L.; Kijung, Y., *Nanotechnology* **2012,** *23,* 194014; h) Liu, B.; Wu, C.-H.; Miao, J.; Yang, P., *ACS Nano* **2014,** *8,* 11739; i) Huang, M. H.; Mao, S.; Feick, H.; Yan, H.; Wu, Y.; Kind, H.; Weber, E.; Russo, R.; Yang, P., *Science* **2001,** *292,* 1897; j) Pauzauskie, P. J.; Sirbuly, D. J.; Yang, P., *Phys. Rev. Lett.* **2006,** *96,* 143903.

[10] Chen, P.-C.; Shen, G.; Shi, Y.; Chen, H.; Zhou, C., *ACS Nano* **2010,** *4,* 4403.

[11] Wagner, R. S.; Ellis, W. C., *Trans. Metall. Aime* **1965,** *233,* 1053.

[12] Chang, J. H.; Chiang, K. M.; Kang, H. W.; Chi, W. J.; Chang, J. H.; Wu, C. I.; Lin, H. W., *Nanoscale* **2015,** *7,* 4572.

[13] a) Glynn, C.; Aureau, D.; Collins, G.; O'Hanlon, S.; Etcheberry, A.; O'Dwyer, C., *Nanoscale* **2015,** *7*, 20227; b) O'Hanlon, S.; Glynn, C.; O'Dwyer, C., *ECS J. Solid State Sci. Technol.* **2015,** *5*, R3100.
[14] Zhu, Z. T.; Menard, E.; Hurley, K.; Nuzzo, R. G.; Rogers, J. A., *Appl. Phys. Lett.* **2005,** *86*, 133507.
[15] a) Glynn, C.; Creedon, D.; Geaney, H.; O'Connell, J.; Holmes, J. D.; O'Dwyer, C., *ACS Appl. Mater. Interfaces* **2014,** *6*, 2031; b) Glynn, C.; Creedon, D.; Geaney, H.; Armstrong, E.; Collins, T.; Morris, M. A.; O'Dwyer, C., *Sci. Rep.* **2015,** *5*, 11574.
[16] Pelletier, O.; Davidson, P.; Bourgaux, C.; Coulon, C.; Regnault, S.; Livage, J., *Langmuir* **2000,** *16*, 5295.
[17] Evans, H., *Mineral. Mag.* **1991,** *55*, 509.
[18] Geaney, H.; Kennedy, T.; Dickinson, C.; Mullane, E.; Singh, A.; Laffir, F.; Ryan, K. M., *Chem. Mater.* **2012,** *24*, 2204.
[19] de Waal, D., *Mater. Res. Bull.* **1991,** *26*, 893.
[20] a) Fukata, N.; Oshima, T.; Okada, N.; Kizuka, T.; Tsurui, T.; Ito, S.; Murakami, K., *Physica B* **2006,** *376-377*, 864; b) Viera, G.; Huet, S.; Boufendi, L., *J. Appl. Phys.* **2001,** *90*, 4175.
[21] Seetharaman, S.; Bhat, H. L.; Narayanan, P. S., *J. Raman Spectrosc.* **1983,** *14*, 401.

Table of Contents Entry:

Contact inter-diffusion allows solid-state ternary metal oxide nanowire growth directly from thin film coated surfaces and devices. Formation and crystallization of complex oxide nanowires on surfaces and devices is facilitated between a solution processed surface oxide film and contacted glass containing a diffusion species. Contact inter-diffusion opens up a new avenue for oxide nanowire research and application to a variety of surfaces and substrates.

Keyword: Contact Inter-diffusion

Growing Oxide Nanowires and Nanowire Networks by Solid State Contact Diffusion into Solution-Processed Thin Films

Colm Glynn, David McNulty, Hugh Geaney and Colm O'Dwyer

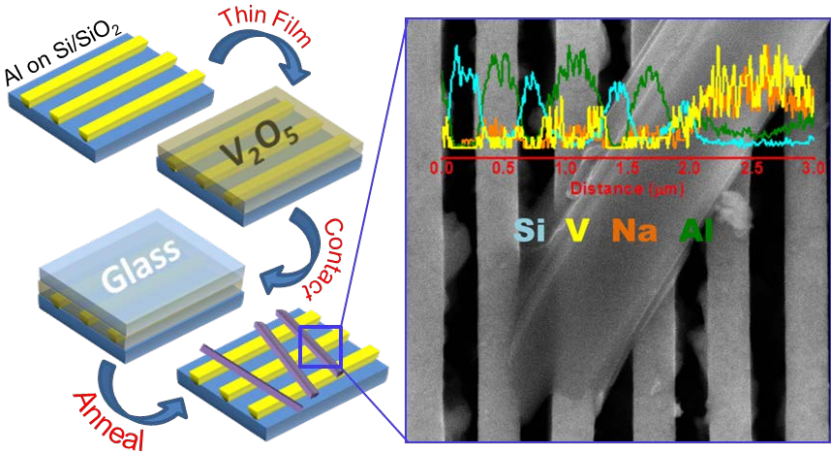

Supporting Information

Growing Oxide Nanowires and Nanowire Networks by Solid State Contact Diffusion into Solution-Processed Thin Films

Colm Glynn, David McNulty, Hugh Geaney and Colm O'Dwyer

FTO Substrates Before and After a-V_2O_5 Coatings

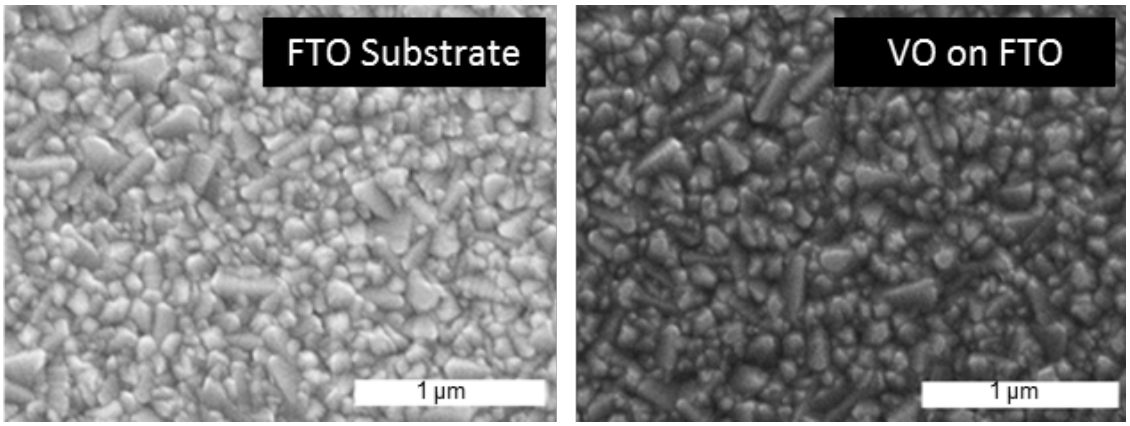

Figure S1. SEM images of the uncoated FTO substrate and a conformal dip-coated VO thin film coating on FTO. The SEM settings (working distance, contrast and accelerating voltage) were kept consistent during acquisition of both images.

NW Formation on Single Layer a-V_2O_5

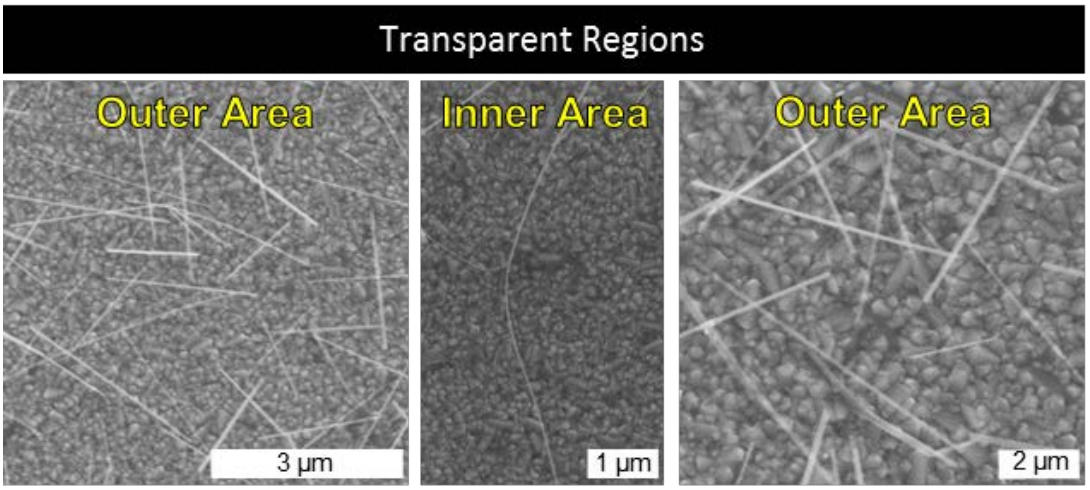

Figure S2. SEM images of NW mesh formed on single a-V_2O_5 layer formed at 300 oC for 12 hours showing disparity of NWs in outer and inner areas.

The NWs formed in the transparent region of Figure 1 (b) are spread across the surface of the transparent region in different concentrations. The outer areas of the transparent region have the highest concentration of NWs while the inner regions have a lower concentration. Surface SEM images of the inner and outer regions are shown in Figure S2 which shows coverage of the FTO substrates of long NWs with random orientations across the surface.

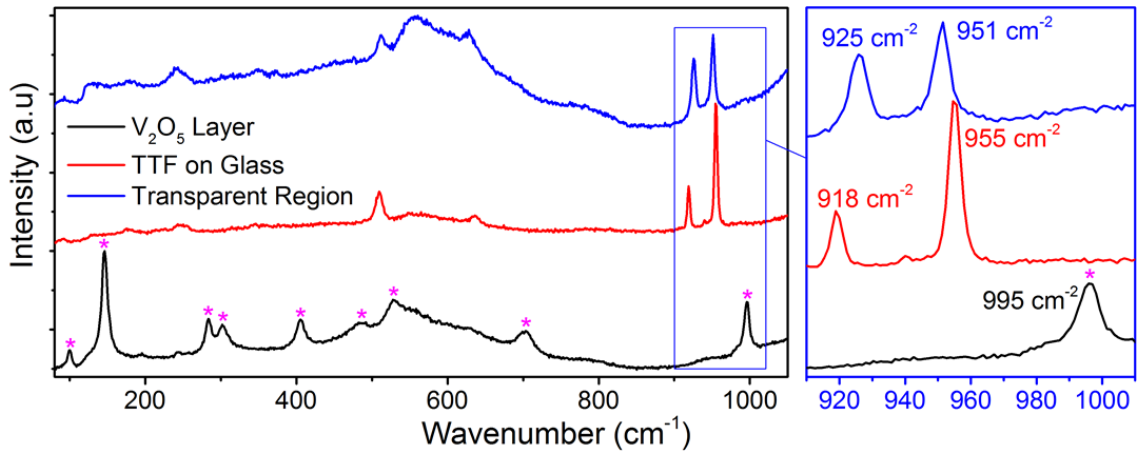

Figure S3. Raman scattering spectra for the NW network formed on a single layer of a-V_2O_5 annealed for 72 hrs at 300 ^oC. NW meshes form in the regions contacted with borosilicate glass while orthorhombic V_2O_5 (vibrations marked with *) forms in the uncontacted regions. Spectra for α-$NaVO_3$ TTF formed on the surface of borosilicate glass is included.

The Raman scattering spectra for the V_2O_5 and transparent regions is shown in supporting information Figure S2. The un-contacted a-V_2O_5 thin film forms the characteristic orthorhombic crystal structure expected from V_2O_5 after annealing.[1] The Raman spectra for α-$NaVO_3$ transparent thin film (TTF) formed on the surface of borosilicate glass is included in Figure S3. The transparent region shows the formation of the characteristic vibrational modes for α-$NaVO_3$. However, the modes are shifted from 918 cm^{-1} and 955 cm^{-1} to 925 cm^{-1} and 951 cm^{-1} respectively which are related to size and stress effects on the crystalline α-$NaVO_3$ phase that forms within the glassy matrix, a common effect for NW systems due to phonon confinement and scattering.[2-3]

NW Formation on Triple Layer a-V_2O_5

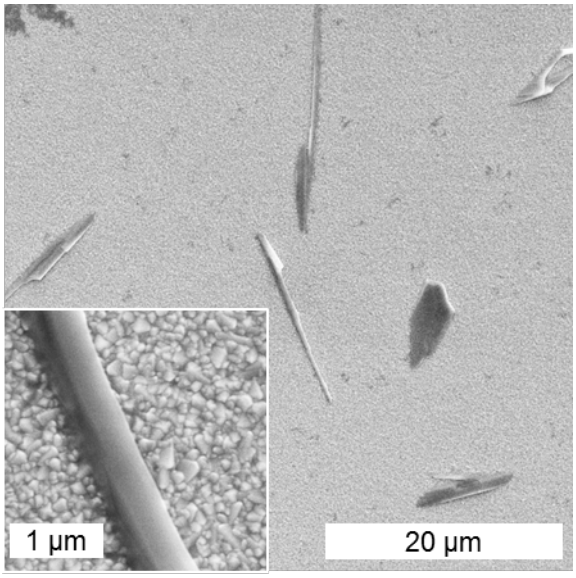

Figure S4. SEM images of interdiffused shards within the transparent region.

Raman Scattering Spectra of Contacted Donor Glass

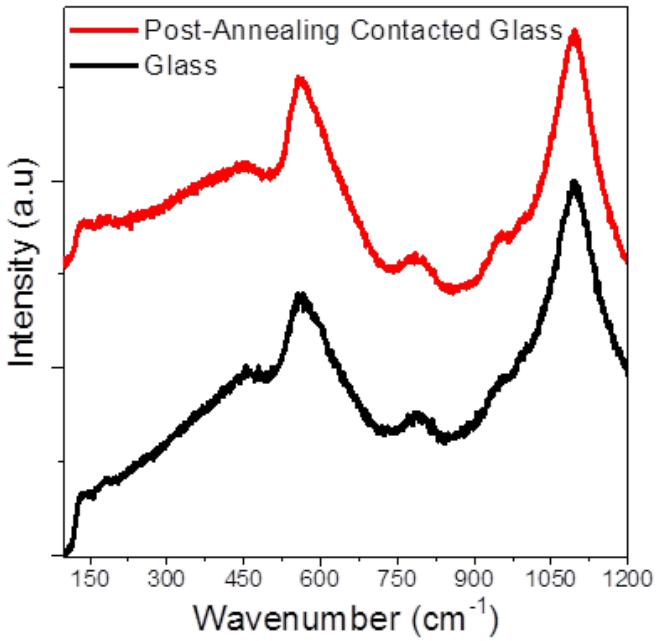

Figure S5. Raman scattering spectra of the donor glass both pre- and post-annealing.

Crosshatch Cut Donor Glass Contact Diffusion

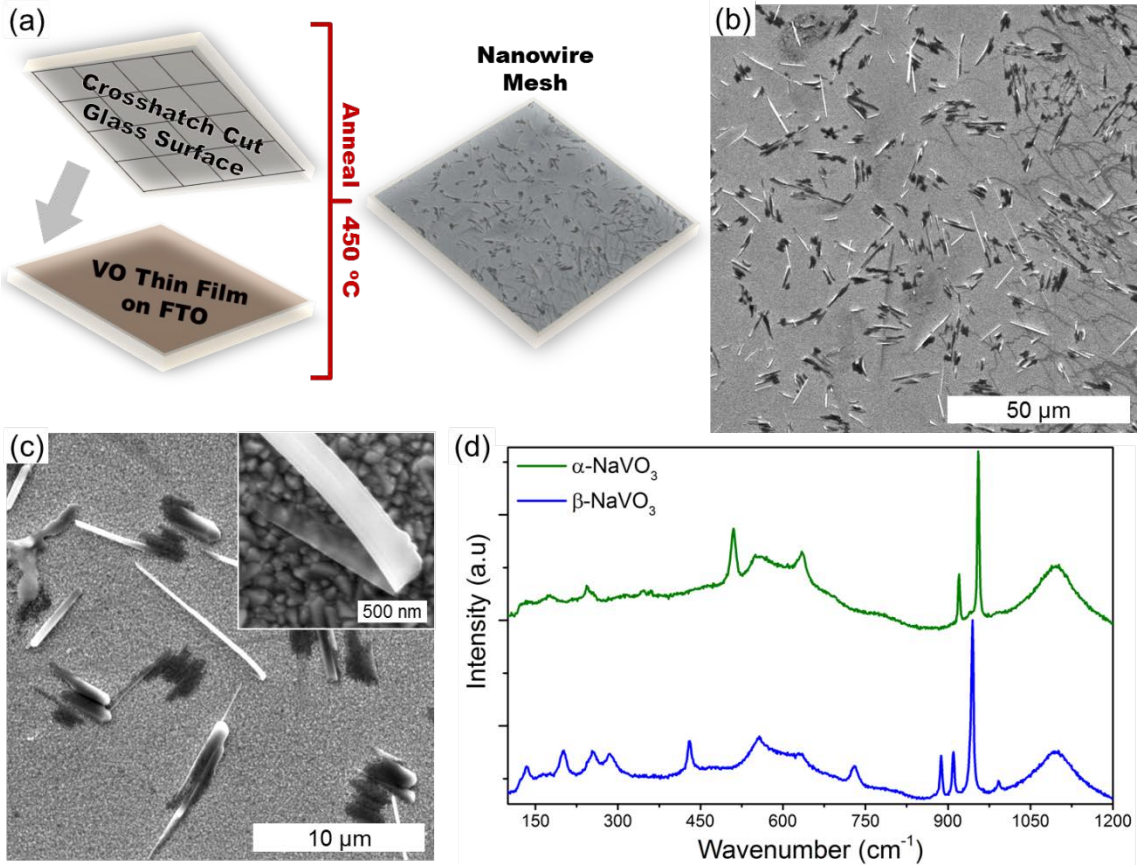

Figure S6. (a) Schematic detailing the large scale formation of NW networks through inter-diffusion processes by utilising a crosshatch cut donor glass. (b) SEM image of the resultant inter-diffused NW network and (c) zoomed in images showing the morphology of the NWs and shards. (d) Raman scattering spectra for two different regions on the surface showing α-$NaVO_3$ and β-$NaVO_3$ formation.

Supporting Information Figure S6 (a) illustrates a technique for the formation of larger nanostructures through contact inter-diffusion by utilising a scribed crosshatch pattern on the donor glass prior to contacting and annealing. The SEM images in the Supporting Information Figure S6 (b, c) show the surface morphology of the NW network formed using the crosshatched donor glass after heating at 450 ^{o}C. The Raman scattering spectra for two different regions of the NW network is shown in the Supporting Information Figure S6 (d) where the vibrational spectra for both α-$NaVO_3$ and β-$NaVO_3$ are present. The cross-hatched contact diffusion source glass spread the pressure exerted on the V_2O_5 thin film equally compared to a conformal source glass. By crosshatching the donor glass, the formation of

larger nanostructures is achieved, however, a large-scale connected network is not achieved which limits the application of the technique suggesting that a planar donor surface is required for high concentration $NaVO_3$ NW networks.

a-V_2O_5 Deposition on Si_3N_4 TEM Grids

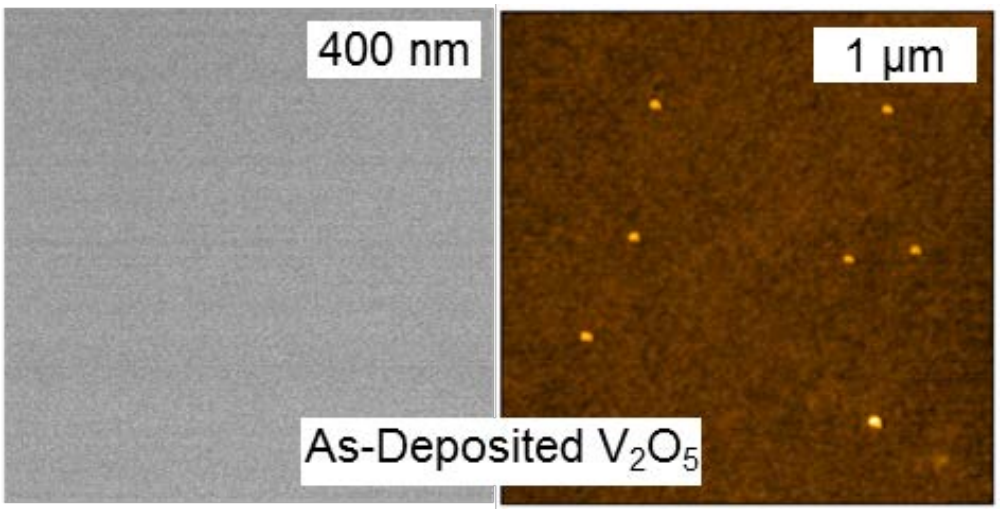

Figure S7. TEM and AFM images of a-V_2O_5 deposited on Si_3N_4 TEM grid prior to annealing.

EDX Mapping interdigitated Al on Si/SiO_2 with V_2O_5/$NaVO_3$ Deposits

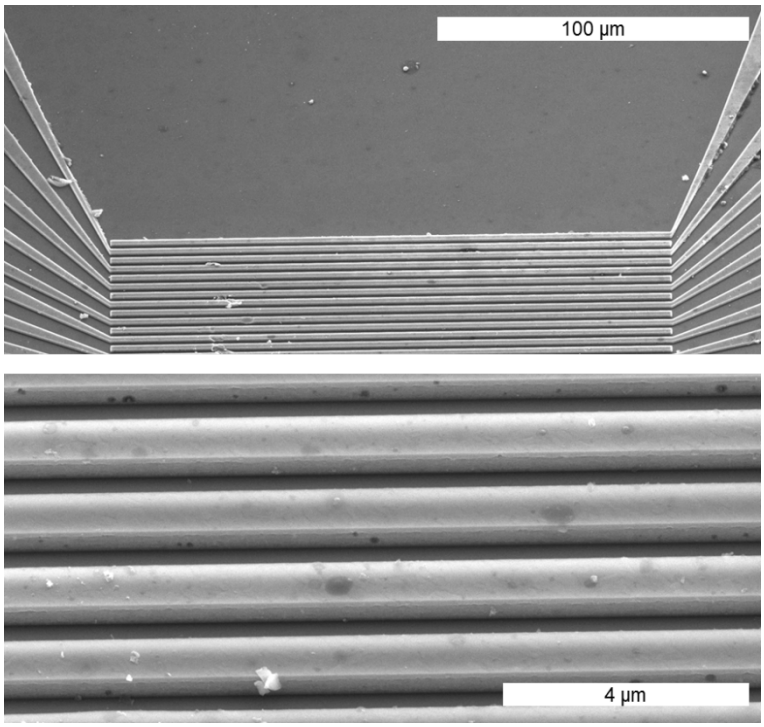

Figure S8. Angled SEM images of interdigitated Al electrodes on Si/SiO_2 substrate.

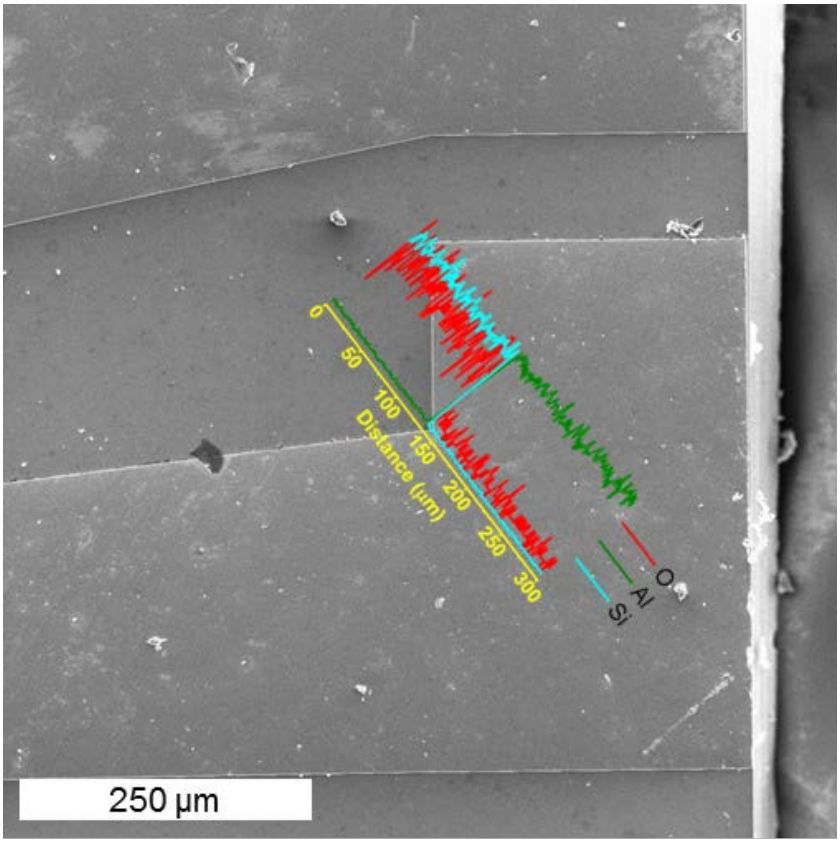

Figure S9. EDX mapping of Al electrode contact on top of Si/SiO_2 substrate.

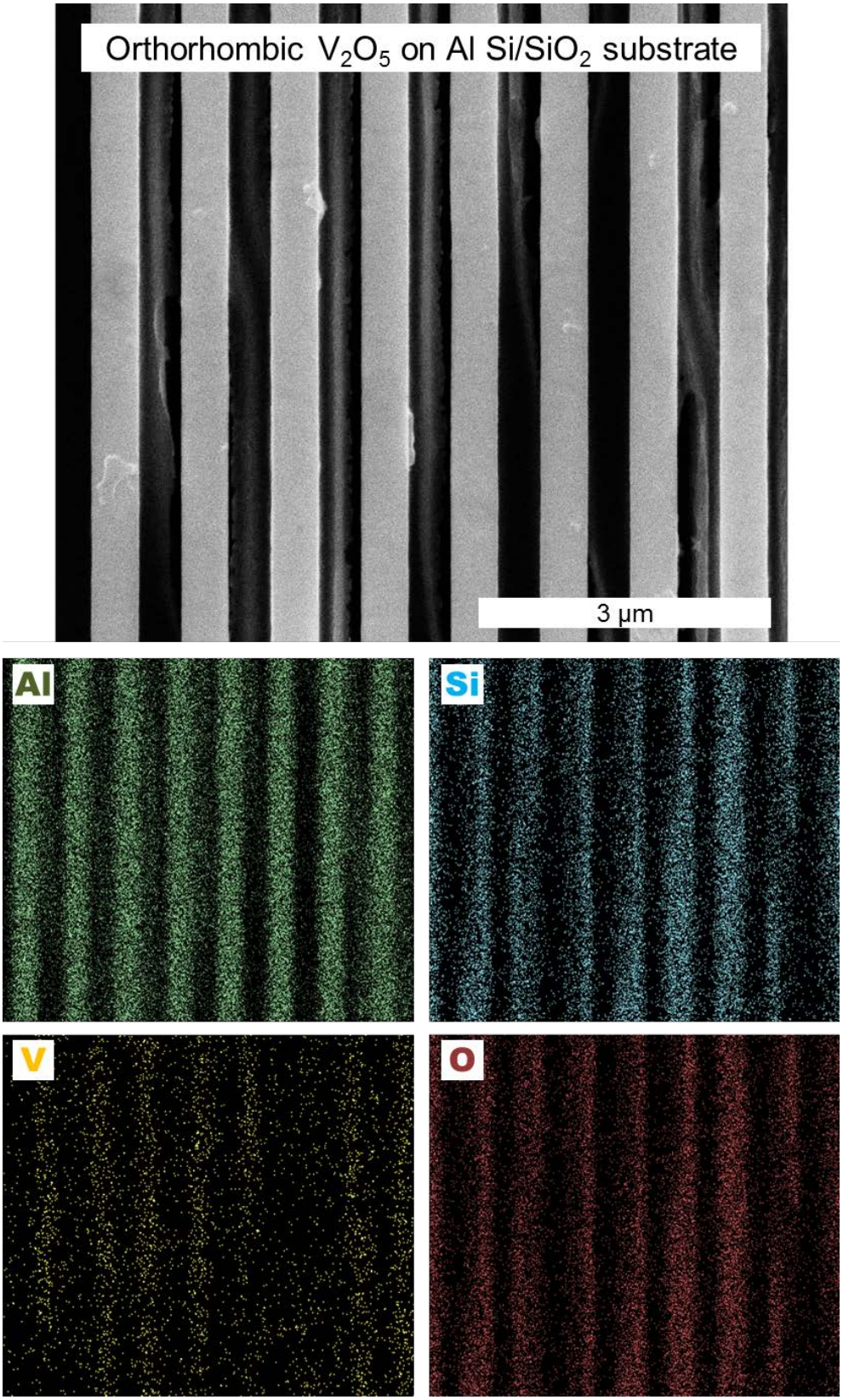

Figure S10. Full EDX maps of orthorhombic V_2O_5 thin film on interdigitated Al electrodes on Si/SiO_2 substrates showing O, V, Al and Si distributions.

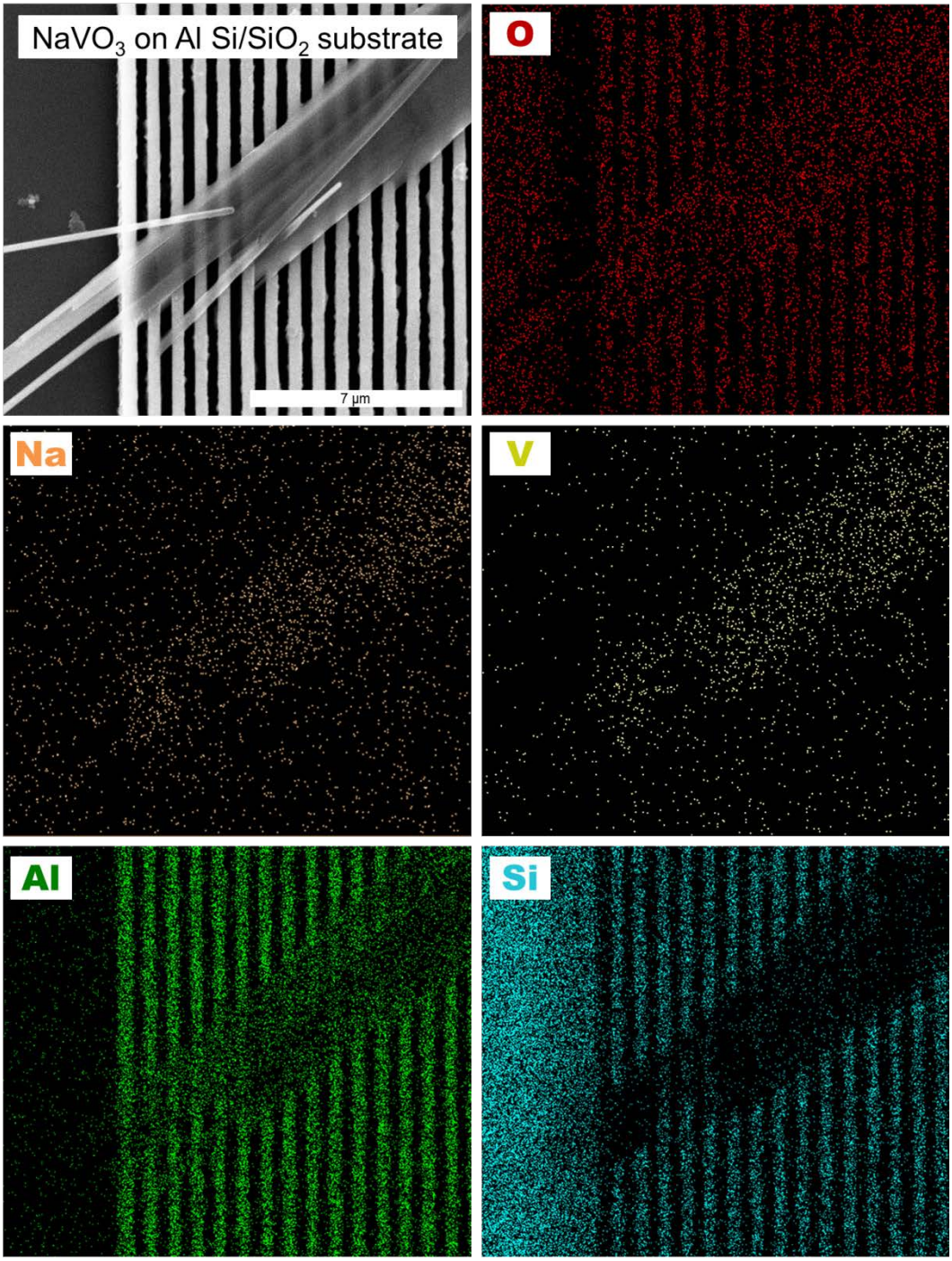

Figure S11. Full EDX maps of $NaVO_3$ NWs on interdigitated Al electrodes on Si/SiO_2 substrates showing O, Na, V, Al and Si distributions.

Supporting Information References

[1] C. Glynn, D. Creedon, H. Geaney, E. Armstrong, T. Collins, M. A. Morris, C. O'Dwyer, *Sci. Rep.* **2015**, 5, 11574.
[2] N. Fukata, T. Oshima, N. Okada, T. Kizuka, T. Tsurui, S. Ito, K. Murakami, *Physica B* **2006**, 376-377, 864.
[3] G. Viera, S. Huet, L. Boufendi, *J. Appl. Phys.* **2001**, 90, 4175.